Heliyon 10 (2024) e27754

Contents lists available at ScienceDirect

Heliyon

journal homepage: www.cell.com/heliyon

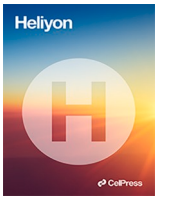

Research article

Novel biomarkers related to oxidative stress and immunity in chronic kidney disease

Fang Bai [a,c,1], Chunjie Wang [a,c], Xin Fan [a], Lin Fang [a], Luyao Li [a], Xiaoning Zhang [d], Kuipeng Yu [a,b,c], Lei Liu [a,b], Ling Guo [a,b,**], Xiangdong Yang [a,b,*]

[a] Department of Nephrology, Qilu Hospital of Shandong University, Jinan, 250012, Shandong, China
[b] Department of Blood Purification, Qilu Hospital of Shandong University, Jinan, 250012, Shandong, China
[c] Laboratory of Basic Medical Sciences, Qilu Hospital of Shandong University, Jinan, 250012, Shandong, China
[d] Department of Nephrology, Shengli Oilfield Central Hospital, Dongying, 257034, Shandong, China

ARTICLE INFO

Keywords:
Chronic kidney disease
Bioinformatic analysis
WGCNA
Biomarker
NCF2
S100A9
SELL

ABSTRACT

Introduction: The incidence of chronic kidney disease (CKD) has been increasing in recent years, gradually becoming a global health crisis. Due to limited treatment options, novel molecular pathways are urgently required to advance the treatment and diagnosis of CKD.

Materials and methods: The characteristics of differentially expressed genes (DEGs) in CKD patients were analyzed using Gene Expression Omnibus (GEO) database, and genes related to oxidative stress were retrieved from the Genecard database. Subsequently, a comprehensive approach was applied, including immune infiltration analysis, weighted gene co-expression network analysis (WGCNA) and protein-protein interaction (PPI) network analysis, to identify hub genes among differentially expressed immune-related oxidative stress genes (DEIOSGs). Validation of hub genes was performed using an external data set, and diagnostic potential capability was evaluated through receiver operating curve (ROC) analysis. In animal experiments, the expression of hub genes in CKD was confirmed by inducing a CKD model through a 5/6 nephrectomy procedure. Finally, the relationship between these hub genes and clinical characteristics were assessed using the Nephroseq v5 database.

Results: 29 DEIOSGs were identified by comprehensive bioinformatics analysis. PPI analysis screened the hub genes NCF2, S100A9, and SELL. ROC analysis demonstrated excellent diagnostic efficacy. Further validation from other databases and animal experiments confirmed a substantial upregulation in the expression of hub genes in CKD. Additionally, clinical correlation analysis established a clear link between hub gene expression and renal function deterioration.

Conclusions: Our study confirms NCF2, S100A9, and SELL as diagnostic biomarkers associated with immune response and oxidative stress in CKD, suggesting their potential as novel targets for CKD diagnosis and treatment.

* Corresponding author. Department of Nephrology, Qilu Hospital of Shandong University, Jinan, 250012, Shandong, China.
** Corresponding author. Department of Nephrology, Qilu Hospital of Shandong University, Jinan, 250012, Shandong, China.
E-mail addresses: gulixiji@sdu.edu.cn (L. Guo), yxd@email.sdu.edu.cn (X. Yang).
[1] First author: Fang Bai.

https://doi.org/10.1016/j.heliyon.2024.e27754
Received 27 February 2024; Accepted 6 March 2024
Available online 12 March 2024

1. Introduction

Chronic kidney disease (CKD) is a worldwide public health concern, and its incidence has been on the rise in recent years, eventually advancing to end-stage renal disease (ESRD) [1,2]. However, the precise process behind CKD advancement remains uncertain, with limited and non-specific treatment options [3,4]. Consequently, delving into the underlying mechanisms and investigating diagnostic biomarkers is critical for the early diagnosis and therapy of CKD.

CKD is usually accompanied by a variety of complex physiological and immunological changes, in which oxidative stress and abnormalities in the immune system play a key role [5]. Oxidative stress plays a crucial part in CKD, resulting from an imbalance between free radicals and antioxidants, potentially harming cells and tissues [6]. In patients with CKD, the degree of oxidative stress is usually elevated, partly due to factors such as inflammation, hypertension, and metabolic disorders [7,8]. Oxidative stress can lead to the generation of oxygen free radicals in renal tissues, triggering cellular damage, fibrosis, and inflammatory responses [9]. The immune system also plays a vital role in the process of CKD, as patients with CKD are usually in the state of immunosuppressed state and are more susceptible to infection [10]. Inflammatory reactions are widespread in CKD patients, they usually exhibit abnormal immune responses [11]. Additionally, autoimmune disorders are more common in patients with CKD, possibly due to disturbances in the immune system [12]. Confirming these relationships require consideration of factors such as the immune response at the cellular and molecular levels, the release of inflammatory mediators, and the mechanisms of oxidative stress. Therefore, treatment and management of CKD requires more comprehensive approaches, addressing these factors to prevent and mitigate complications and enhance patients' quality of life [13].

In this study, we determined the diagnostic genes of CKD by combining the bioinformatics method of immune infiltration and oxidative stress. We further validated these results using external data sets and animal experiments in order to better understand the underlying molecular processes in CKD development.

2. Materials and methods

2.1. Data source

In this investigation, the gene expression microarray data was obtained from the Gene Expression Omnibus (GEO) database (http://

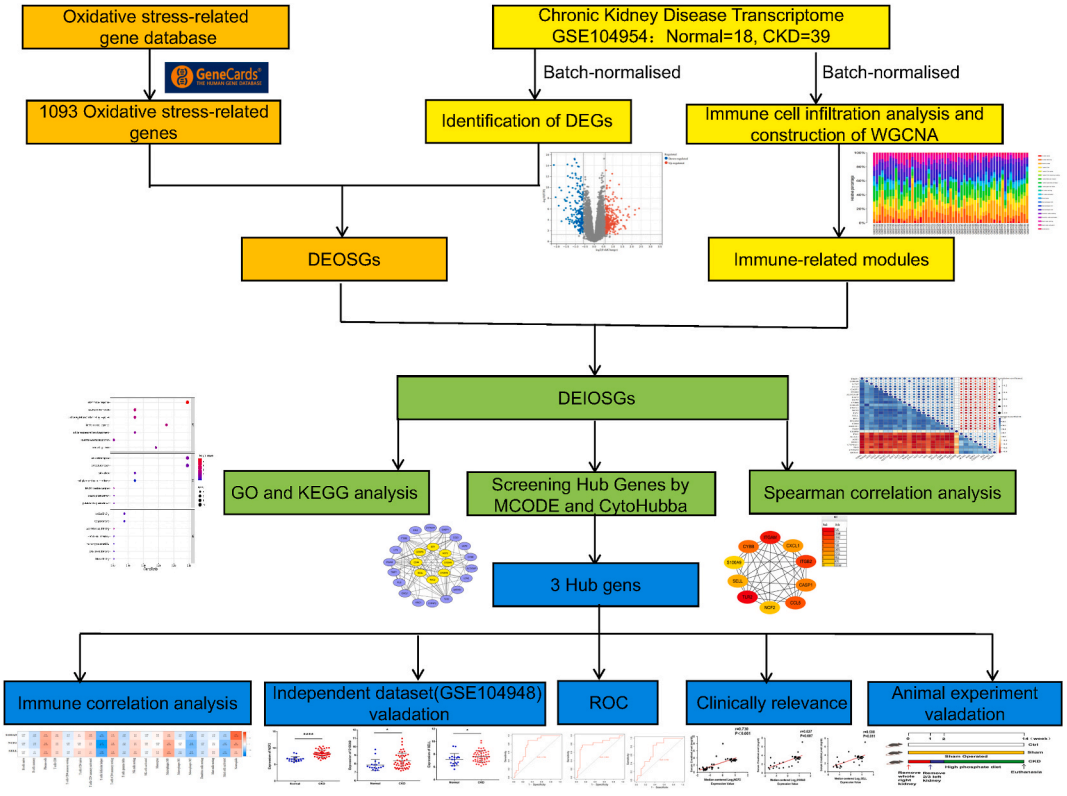

Fig. 1. Flowchart for comprehensive bioinformatics analysis and validation experiment of CKD. DEGs, differentially expressed genes; WGCNA, weighted gene co-expression network analysis; DEOSGs, differentially expressed oxidative stress-related genes; DEIOSGs, differentially expressed immune-related oxidative stress genes; GO, gene ontology; KEGG, kyoto encyclopedia of genes and genomes; ROC, receiver operating curve.

www.ncbi.nlm.nih.gov/geo). The data set GSE104954 (platform GPL22945, Affymetrix Human Genome U133 Plus 2.0) included information from 39 individuals with CKD (GSM2811029-GSM2811042, GSM2811061-GSM2811085) and 18 control human kidney samples (GSM2811043-GSM2811060). The gene expression profiles of CKD patients encompassed individuals with diabetic nephropathy (DN; n = 7), focal segmental glomerulosclerosis (FSGS; n = 7), minimal Change Disease (MCD; n = 4), and ANCA-associated glomerulonephritis (RPGN; n = 21) (Additional file 1: table S1). For validation, the data set GSE104948 (platform GPL22945, Affymetrix Human Genome U133 Plus 2.0) contained information from 50 individuals with CKD (GSM2810770-GSM2810792, GSM2810811-GSM2810837) and 18 control human kidney samples (GSM2810793-GSM2810810) was used. Batch normalization of the raw data was performed using the "limma" package [14] within the R software. Fig. 1 illustrates the study's design details visually.

Simultaneously, we retrieved 1093 genes associated with oxidative stress from the GeneCards database (https://www.genecards.org) by searching for the term "oxidative stress." The screening threshold was a relevance score of ≥7 (Additional file 2: table S2).

2.2. Differentially expressed gene analysis

The replicability of the GSE104954 data set was evaluated using the Uniform manifold approximation and projection (UMAP) technique. Differentially expressed genes (DEGs) were identified with an adj. P-value <0.05 and $|\text{Log}_2\text{fold change}| > 0.5$ through the "limma" package. Heatmaps were generated using the "pheatmap" package in R, while the volcano plots and box plots were produced using the Sangerbox tools, an online platform for data analysis available at http://vip.sangerbox.com/home.html.

2.3. Immune infiltration analysis and construction of weighted gene co-expression networks

The CIBERSORT algorithm [15] was employed to determine the proportions of the 22 distinct immune cell types in the samples from GSE104954. Weighted gene co-expression network analysis (WGCNA) was used to identify cohesive gene networks and their interplay, and their connections with external sample traits that could potentially indicate biomarkers or therapeutic targets.

In our study, modules closely associated with immune cells in CKD patients were constructed using the R package "WGCNA" [16]. Initially, the sample data and outliers were processed. Subsequently, the 'WGCNA' software created a correlation matrix with a soft-thresholding power of 8 and a correlation coefficient threshold of 0.83. The correlation matrix was converted into an adjacency matrix, generating a topological overlap matrix (TOM). Hierarchical clustering with average linkage on genes, based on the TOM-based phase dissimilarity metric, was performed to reveal similar expression patterns, grouping them into distinct gene modules.

For further analysis, our focus was on genes within modules that exhibited strong associations with infiltrated immune cells (correlation ≥0.6 and P-value <0.05). Differentially expressed immune-related oxidative stress genes (DEIOSGs) were identified by integrating genes obtained from both WGCNA and the analysis of differentially expressed oxidative stress-related genes (DEOSGs).

2.4. Gene function and correlation analysis

Enrichment analyses were conducted for DEIOSGs. Gene Ontology (GO) and Kyoto Encyclopedia of Genes and Genomes (KEGG) pathway enrichment analyses were performed using DAVID version 6.8 (https://david.ncifcrf.gov/conversion.jsp), a widely used tool in bioinformatics research for comprehensive gene and protein function analysis and categorization. The GO analysis covered three aspects: cellular composition (CC), biological process (BP), and molecular function (MF). The analysis outcomes and visualizations were presented using https://www.bioinformatics.com.cn, a freely accessible online platform designed for data exploration.

2.5. Protein–protein interaction network construction

The STRING database was employed to analyze the protein-protein interaction (PPI) networks associated with modules. Visualization of these PPI networks was achieved using Cytoscape Software (version 3.8.2). For a more detailed exploration of the principal functional modules, the MCODE plug-in within Cytoscape was utilized. Furthermore, the Maximum Clique Centrality (MCC) algorithm was employed by the cytoHubba plugin in Cytoscape to assign scores to each node genes, evaluating their network centrality. The top 10 nodal genes based on the MCC score from each algorithm were selected as pivot genes. To identify the hub gene, a cross-linking process was conducted on the top-scoring genes from both MCODE and CytoHubba. Additionally, we utilized https://www.bioinformatics.com.cn to generate a receiver operating curve (ROC), assessing capability of hub genes in distinguishing CKD patients from healthy controls.

2.6. Hub genes validation and correlation analysis with renal function

The variance in gene expression of hub genes between CKD and healthy renal samples was confirmed by examining the GSE104948 data set. Subsequently, the relationship between hub gene expression and clinical traits was assessed using data from the Nephroseq v5 online database (http://v5.nephroseq.org) and statistical analysis was performed.

2.7. Animal models

Twelve male C57BL/6 mice of wild-type strain at 8 weeks of age were obtained from the Animal Experiment Center at Shandong University in Jinan, China. The mice were distributed into three groups, with four mice each in the control group (Ctrl), sham

operation group (Sham), and chronic kidney disease group (CKD). CKD mice were induced with 5/6 nephrectomy (5/6Nx) as previously described [17]. The experimental procedure entailed a two-step nephrectomy. Specifically, the entire right kidney was removed, followed by a one-week interval, and then a section of the functional left kidney was preserved, while the rest was excised. This preserved segment was then returned to its original position. The sham group underwent sham surgeries, involving exposure and gentle handling of the relevant kidney without any further intervention.

After one week, mice were subjected to a diet containing 1.0% phosphorus for 4 weeks, followed by a 2.0% phosphorus diet for 8 weeks. Euthanasia was conducted by administering an overdose of isoflurane followed by cervical dislocation. Kidney tissue was collected and either fixed for Masson and HE staining or promptly frozen in liquid nitrogen and stored at −80 °C for subsequent investigations. All protocols adhered to the guidelines sanctioned by the Animal Care and Use Committee of Shandong University.

2.8. Renal function analysis

The levels of serum creatinine (SCr) and blood urea nitrogen (BUN) were determined by utilizing a Creatinine Assay Kit and a BUN kit (Nanjing Jiancheng Bioengineering Institute, Nanjing, China), respectively, in accordance with the instructions provided by the manufacturer.

2.9. RNA extraction and RT-qPCR analysis

Mouse kidney tissue was used to isolate total RNA using the RNAfast200 Kit (Fastagen). Subsequently, cDNA synthesis was performed using the SureScriptTM First-Strand cDNA Synthesis Kit (QP056T, GeneCopoeia). Real-time quantitative polymerase chain reaction (RT-qPCR) was conducted using the Bio-Rad CFX PCR System (Bio-Rad) with the SYBR Green reagent (1725201, Bio-Rad). The procedure was repeated thrice for each sample. The exact primer sequences are provided in Table 1. The $2^{-\Delta\Delta Ct}$ method was employed for gene expression analysis, and the expression levels were standardized with respect to GAPDH.

2.10. Protein extraction and western blotting analysis

Total proteins were extracted from mouse kidney tissue using radioimmunoprecipitation assay (RIPA) buffer (P0013D, Beyotime) supplemented with 1% phenylmethylsulfonyl fluoride (PMSF) (329-98-6, Solarbio). Protein quantification was performed using Bio-RAD kits. The protein samples were treated uniformly and then subjected to 10% SDS-PAGE analysis. Subsequently, the proteins were transferred onto PVDF membranes and blocked with 5% skim milk. Primary antibodies targeting NCF2 (1:1000 dilution, Cat.109366, Abcam), S100A9 (1:1000 dilution, Cat.242945, Abcam), SELL (1:1000 dilution, Cat.PB9389, Boster), and GAPDH (1:6000 dilution, Cat. 60004-1-Ig, ProteinTech) were incubated overnight at 4 °C. After washing, the proteins were exposed to a horseradish peroxidase-conjugated secondary antibody (1:6000 dilution, Cat.SA00001-2, ProteinTech) for 1 h at room temperature. The bands were visualized using an enhanced chemiluminescence (ECL) system, and the signal intensity was measured using ImageJ software.

2.11. HE and masson staining

The kidneys were fixed, embedded, and sectioned into 4 mm thick slices. The morphology of renal tissue was examined by utilizing the HE Staining Kit (Solarbio, Beijing, China). Renal fibrosis was observed by utilizing a customized Masson's trichrome staining kit (Solarbio, Beijing, China) with the aid of a light microscope (Olympus, Tokyo, Japan). The HE and Masson staining protocols were carried out in accordance with the instructions provided by the manufacturer.

2.12. Immunohistochemical staining

The mouse kidney tissue sections were stained using primary antibodies that targeted NCF2 (1:1000 dilution, Cat.109366, Abcam), S100A9 (1:1000 dilution, Cat.242945, Abcam), SELL (1:1000 dilution, Cat.PB9389, Boster), and GAPDH (1: 6000 dilution, Cat.60004-1-Ig, ProteinTech) at 4 °C overnight. The identification and cultivation followed the typical two-step procedure, and immunohistochemical staining was accomplished using the 3, 3′-diaminobenzidine (DAB) chromogenic kit. The NIS Element software and the Nikon microscope imaging system were used to obtain and analyze the images. The ImageJ software was utilized for conducting quantitative

Table 1
Quantitative PCR primers used in the study.

Primer name	Primer Sequence (from 5′ to 3′)
Mus-NCF2	Forward: 5′-GCTTCGGATTCACCCTCAGT-3′ Reverse: 5′-AGCTTCAGTTCCTTGGGCTC-3′
Mus-S100A9	Forward: 5′-TCAGATGGAGCGCAGCATAA-3′ Reverse: 5′-GGCTTCATTTCTCTTCTCTTTCTTC-3′
Mus-SELL	Forward: 5′-AGCCAATCTGCCAAGAGACA-3’ Reverse: 5′-CCATCCTTTCTTGAGATTTCTTGCC-3′
Mus-GAPDH	Forward: 5′-GCACCGTCAAGGCTGAGAAC-3’ Reverse: 5′-TGGTGAAGACGCCAGTGGA-3′

analysis.

2.13. Statistical analysis

The statistical analysis was performed using GraphPad Prism 8 and R software, specifically version 4.1.3. Two groups were compared using a two-tailed unpaired *t*-test. The level of statistical significance was set at a P-value less than 0.05. Significance levels were denoted as follows: *P < 0.05, **P < 0.01, ***P < 0.001, and ****P < 0.0001, with decreasing probability values.

3. Results

3.1. Identification of DEGs

In order to identify genes linked to CKD, the mRNA expression microarray data (GSE104954) was initially obtained from GEO. Subsequently, the unprocessed microarray data was analyzed and standardized in Fig. 2a. The distribution of CKD and normal samples was visualized in the UMAP results (Fig. 2b). Following that, the analysis of differential gene expression was performed, leading to the discovery of 653 genes that showed significant changes in expression ($|\log_2 FC| > 0.5$ and adjusted $P < 0.05$). Out of these, 278 genes showed a decrease in expression, whereas 375 genes showed an increased expression (Fig. 2c and d). From the Genecard database, an additional 1093 genes associated with oxidative stress were extracted. After comparing these genes with the DEGs, 94 genes were identified to exhibit differential expression and were also linked to oxidative stress (Fig. 2e).

3.2. Immune infiltration analysis and construction of weighted gene co-expression networks

The enrichment fraction of 22 distinct immune infiltrating cell types in both CKD and normal samples was displayed (Additional file 3: fig. S1). There were notable variations ($P < 0.05$) in the composition of immune cells between the CKD and normal samples, with five distinct types showing significant disparities (Fig. 3a). The cell categories included regulatory T cells (Tregs), gamma delta T cells, M1 macrophages, resting mast cells, and activated mast cells.

The sample cluster tree indicated the exclusion of a single anomalous sample (Additional file 4: fig. S2). Subsequently, the optimal

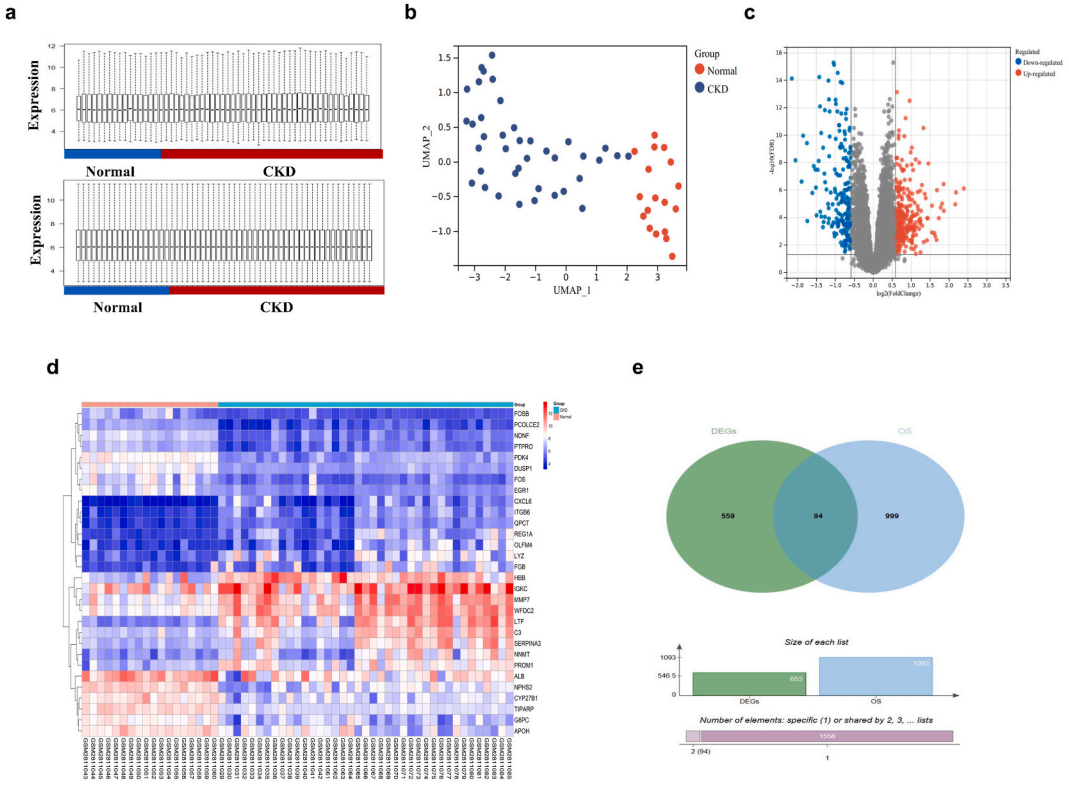

Fig. 2. Detection of DEGs. **a.** Box plot of normalized data from 57 samples. **b.** UMAP for GSE104954. **c.** Volcano plot of DEGs in GSE104954. Upregulated genes were represented by red dots, while downregulated genes were represented by blue dots. **d.** Heatmap of the DEGs in GSE104954. **e.** Exploration of the DEOSGs using Venn diagrams. DEGs, differentially expressed genes; DEOSGs, differentially expressed genes related to oxidative stress.

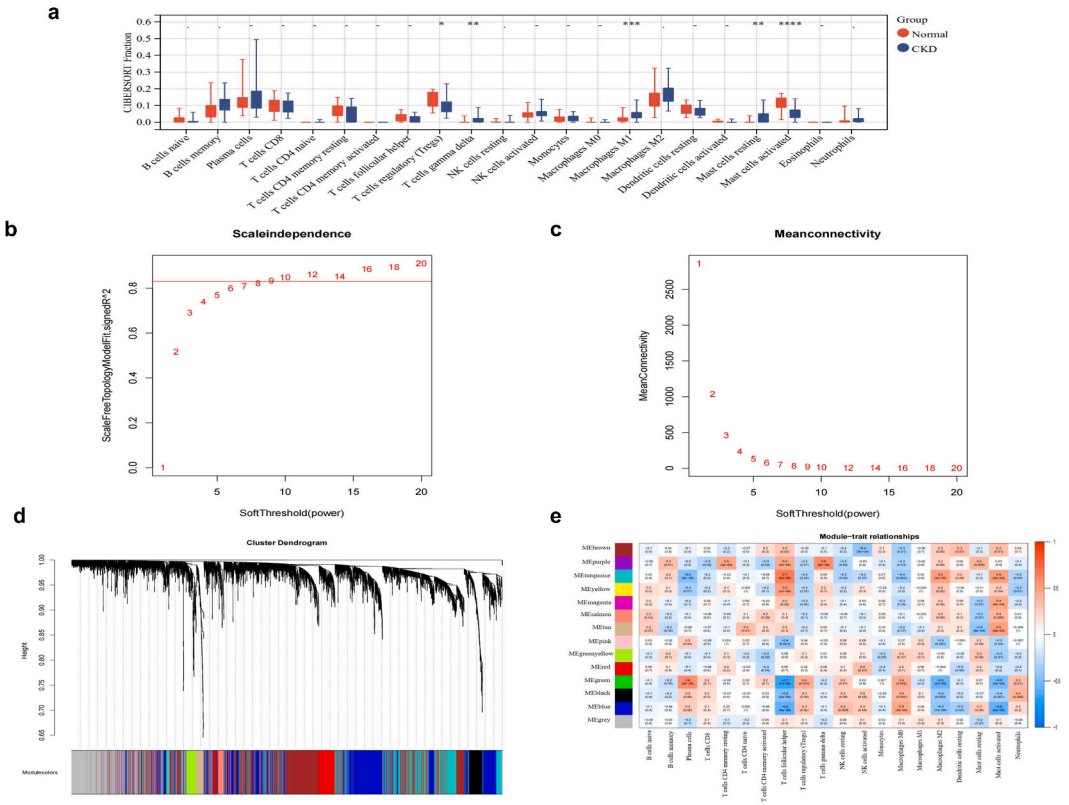

Fig. 3. Immune infiltration analysis and development of weighted gene co-expression networks. a. Box plot of 22 types of immune infiltrating cells in the CKD and normal samples. **b.** Evaluation of fitting indices for scale-free networks across various soft-thresholding powers (β). **c.** Examination of the mean connectivity across different soft-thresholding powers. **d.** Dendrogram based on a dissimilarity metric for DEGs. **e.** Module-trait relationships between WGCNA modules and immune cells. CKD, chronic kidney disease; DEGs, differentially expressed genes.

soft-threshold exponent was determined as 8 through the construction of a scale-free network (Fig. 3b and c). After conducting the WGCNA analysis, a grand total of 14 modules were discovered in this particular investigation (Fig. 3d). Furthermore, the analysis of the relationship between these modules and traits (infiltrated immune cells) revealed that the turquoise module displayed a strong positive correlation with T cells follicular helper (Correlation = 0.7, P-value = 9e-09), the purple module exhibited a significant positive correlation with T cells gamma delta (Correlation = 0.6, P-value = 5e-6), and the green module showed a pronounced positive correlation with Plasma cells (Correlation = 0.6, P-value = 5e-6) (Fig. 3e).

3.3. Identification and functional enrichment analysis of DEIOSGs

Through the integration of genes obtained from both DEOSGs analyses and examination of the turquoise, purple, and green modules, 29 DEIOSGs were discovered (Fig. 4a). Subsequently, a correlation analysis was performed to investigate the relationships in expression among these DEIOSGs (Fig. 4b). Afterwards, GO and KEGG pathways enrichment analyses were performed to explore the functions of DEIOSGs. During the GO analysis, it was discovered that DEIOSGs exhibited strong connections with activities like inflammatory response and neutrophil chemotaxis (biological process), extracellular space and extracellular region (cell component), as well as iron ion binding and receptor binding (molecular function) (Fig. 4c and d; Additional file 5: table S3). Furthermore, the KEGG pathway analysis emphasized the participation of DEIOSGs in Neutrophil extracellular trap formation (Fig. 4e and f; Additional file 6: table S4).

3.4. Identification and validation of hub genes

In order to further explore the primary DEIOSGs linked to CKD and elucidate their underlying mechanisms, the 29 DEIOSGs were utilized to create a PPI network using the online STRING database. There was a total of 26 nodes and 102 edges in the PPI network. Within these 26 nodes, genes with high binding degrees were identified using the MCODE (Fig. 5a) and MCC (Fig. 5b) calculation methods in Cytoscape. The DEIOSGs that play pivotal roles in CKD were subsequently selected through a Venn diagram analysis, NCF2, S100A9, and SELL were revealed as central genes (Fig. 5c). Further details about these hub genes were presented in Table 2.

Concurrently, the levels of expression of three hub genes displayed remarkable diagnostic capability in differentiating CKD patients

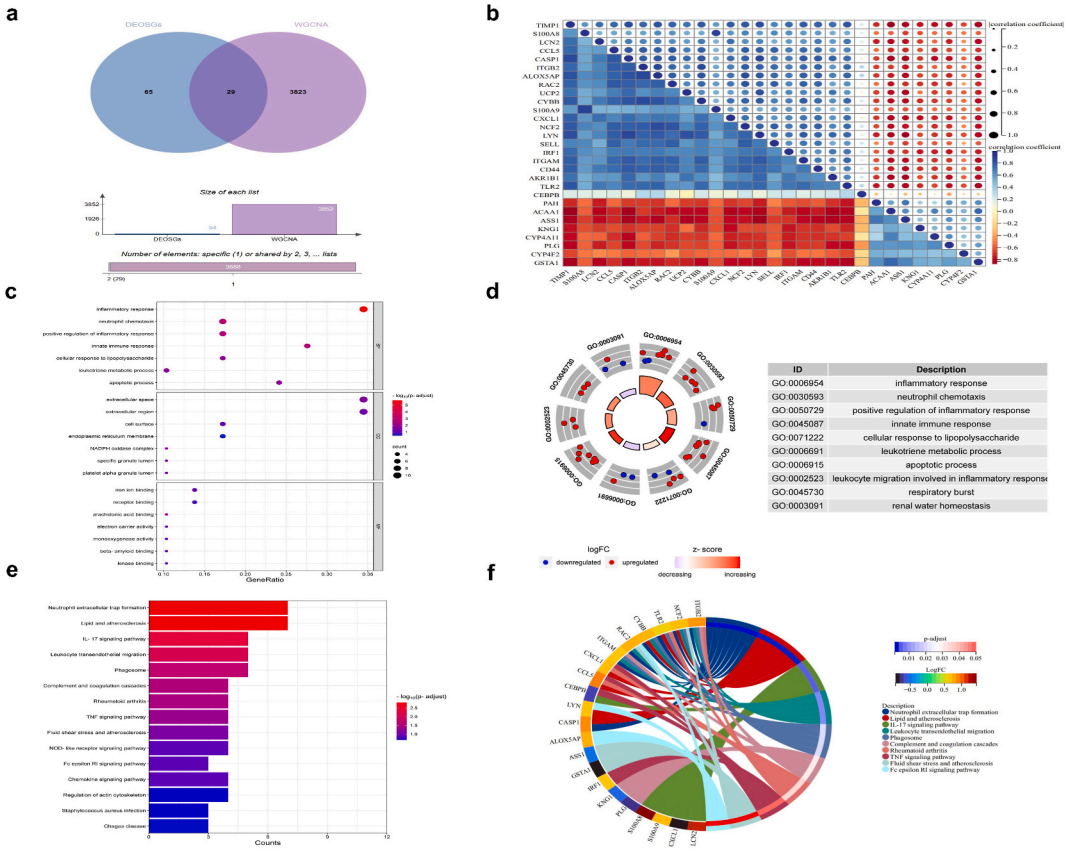

Fig. 4. Procurement and functional enrichment assessment of DEIOSGs. a. Exploration of the DEIOSGs using Venn diagrams. **b.** Spearman's correlation analysis of 29 DEIOSGs. **c.** Bubble plots of the GO enrichment terms. **d.** Circle plot of the GO enrichment terms. **e.** Bar plots of the KEGG enrichment pathways. **f.** Chord plot of the KEGG enrichment pathways. GO, Gene Ontology; KEGG, Kyoto Encyclopedia of Genes and Genomes; BP, biological process; CC, cellular component; MF, molecular function.

from healthy controls was demonstrated by ROC analysis (Fig. 5d–f). Additionally, in order to confirm the altered expression of these three hub genes, an independent data set GSE104948 was utilized to corroborate a significant upregulation in the expression of these hub genes in CKD samples (Fig. 5g–i). Furthermore, Pearson correlation analysis was employed to delve deeper into the potential connection between the expression of hub genes and the prevalence of immune cells. NCF2 expression exhibited a positive correlation with Neutrophil expression, whereas S100A9 and SELL showed a negative correlation with T cells follicular helper expression (Additional file 7: fig. S3).

3.5. Experimental verification of hub genes expression in vivo

To induce CKD animal model, mice were underwent 5/6 nephrectomy and subjected to a high phosphate diet (Fig. 6a). There were no difference between control group and sham-operated group of serum creatinine and blood urea nitrogen. However, in the CKD group, there was a notable increase in both serum creatinine and blood urea nitrogen levels (Fig. 6b–c). Furthermore, HE staining revealed that the renal tissue of sham-operated mice exhibited no apparent changes compared with the control group. In contrast, the renal tissue structure of CKD mice displayed significant damage, including renal tubular dilatation, partial atrophy, and inflammatory cell infiltration. Masson staining further illustrated the substantial deposition of collagen fiber in the CKD group (Fig. 6d).

Compared to the control group, the relative mRNA expression levels of NCF2, S100A9, and SELL in the sham-operated group exhibited no significant changes, while the relative mRNA expression levels of NCF2, S100A9, and SELL in the CKD group were obvously increased (Fig. 6e–g). Additionally, Western blot analysis indicated that, in comparison to the control group, the protein expression levels of NCF2, S100A9, and SELL in the sham-operated group remained relatively unchanged, while the CKD group exhibited higher levels of NCF2, S100A9, and SELL (Fig. 6h and i). Furthermore, immunohistochemistry (IHC) was conducted to preliminarily assess the expression of NCF2, S100A9, and SELL in mouse kidneys. Relative to the control group, the positive staining areas of NCF2, S100A9, and SELL in the sham-operated group showed no significant change, whereas the positive staining areas of NCF2, S100A9, and SELL in the CKD group were larger (Fig. 6j).

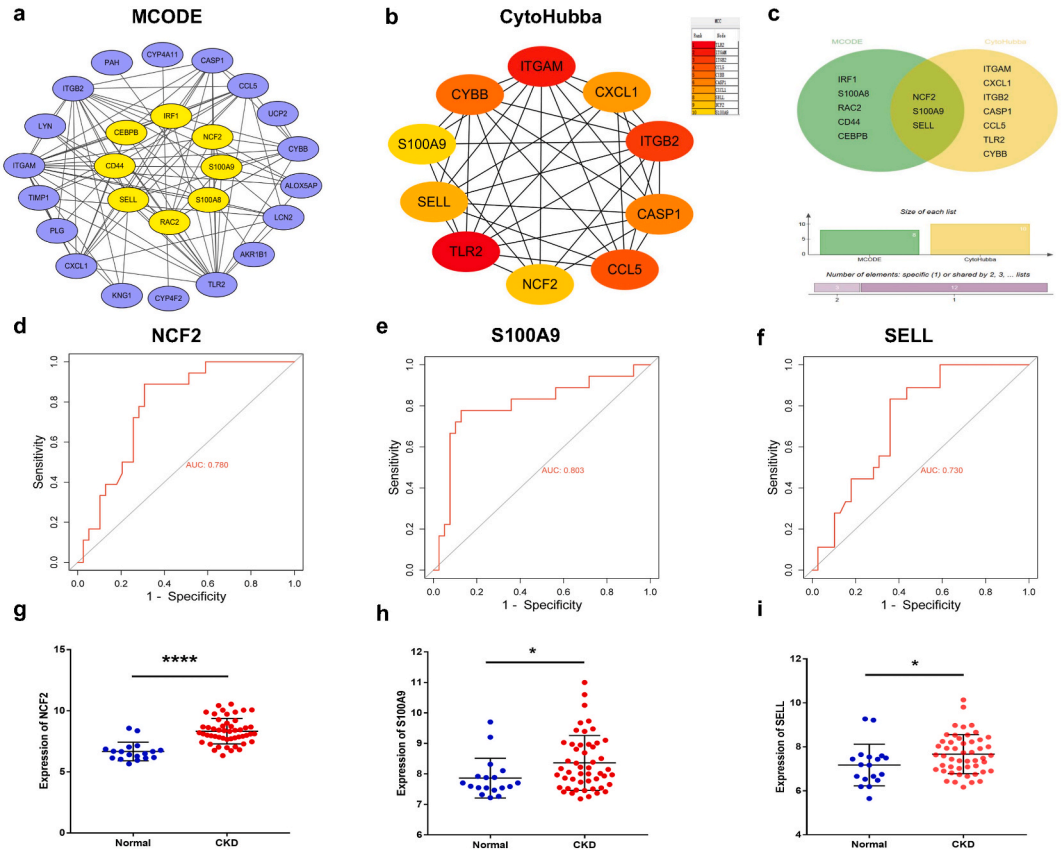

Fig. 5. Screening hub DEIOSGs in CKD and confirming in the GSE104948 database. a. PPI network of hub genes calculated by MCODE algorithm. **b.** PPI network of hub genes calculated by MCC algorithm. **c.** The overlap between the crucial genes identified by MCC and MCODE was displayed through Venn diagram. **d.** ROC curve of NCF2 expression in CKD (AUC = 78.0%). **e.** ROC curve of S100A9 expression in CKD (AUC = 80.3%). **f.** ROC curve of SELL expression in CKD (AUC = 73.0%). **g.** Validation of NCF2 in GSE104948. **h.** Validation of S100A9 in GSE104948. **i.** Validation of SELL in GSE104948.

Table 2
Comprehensive biological roles of biomarkers sourced from the GeneCards database.

Gene name	Biological function	logFC	Adj.P-value
Neutrophil Cytosolic Factor 2 (NCF2)	Activation of the latent NADPH oxidase (necessary for superoxide production).	0.629	0.002
S100 Calcium Binding Protein A9 (S100A9)	Playing a prominent role in the regulation of inflammatory processes and immune response	0.633	0.011
Selectin L (SELL)	Mediating cell adhesion by binding to glycoproteins on neighboring cells	0.594	0.011

3.6. Correlation between the expression of hub genes and clinical databases

The relationship between expression of hub genes and clinical data was validated using multiple data sets from the Nephroseq database. The findings indicated that in the TubInt cohort of IgA nephropathy within Ju CKD, there was a strong association between NCF2 expression and serum creatinine levels ($r = 0.730$, $P < 0.001$, Fig. 7a). In contrast, across all TubInt data sets in Ju CKD, there was a negative correlation between NCF2 expression and glomerular filtration rate (GFR) ($r = -0.503$, $P < 0.001$, Fig. 7b). Similarly, in the TubInt cohort of diabetic nephropathy (DN) in Ju CKD, a direct association was observed between the expression of S100A9 and the levels of serum creatinine ($r = 0.627$, $P = 0.007$, Fig. 7c). On the other hand, across all TubInt data sets within Ju CKD, there was a negative relationship between S100A9 expression and GFR ($r = -0.448$, $P < 0.001$, Fig. 7d). Furthermore, in the TubInt cohort of diabetic nephropathy within Ju CKD, there was a positive correlation between SELL expression and serum creatinine levels ($r = 0.598$, $P = 0.011$, Fig. 7e). Meanwhile, across all TubInt data sets in Ju CKD, there was a negative correlation between SELL expression and GFR ($r = -0.418$, $P < 0.001$, Fig. 7f).

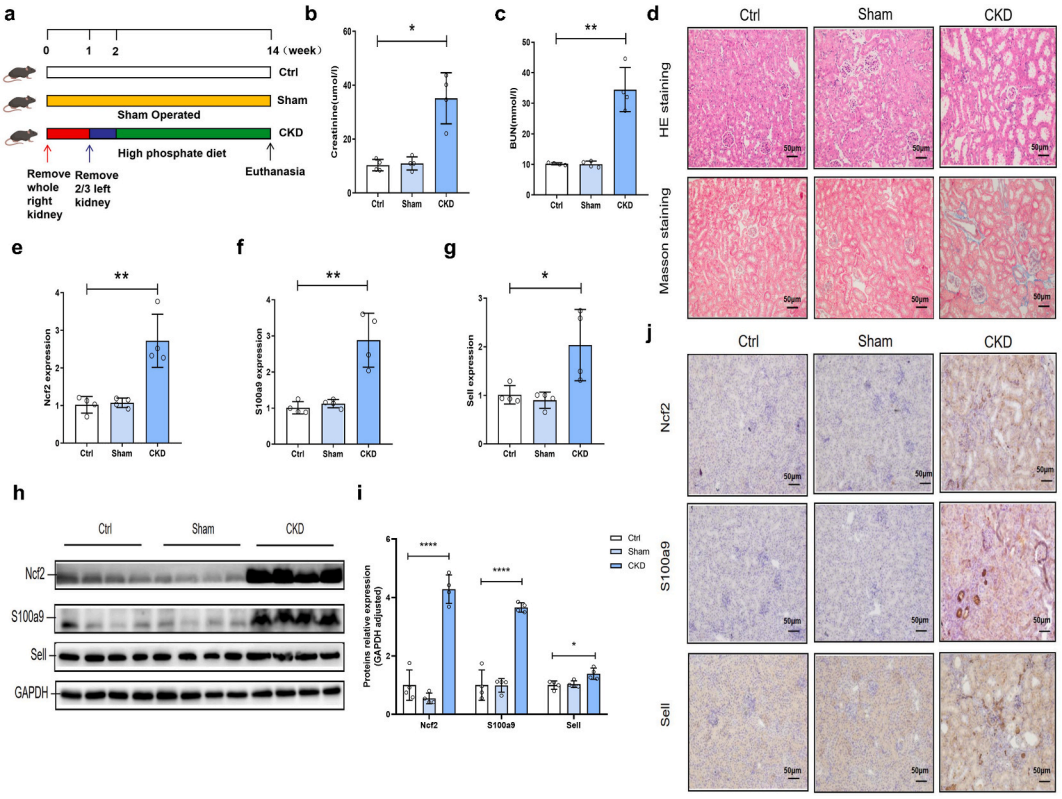

Fig. 6. The expression of hub genes was confirmed in vivo experiments. a. Experimental Design. Mice underwent a two-stage procedure, during which 5/6 of the kidney was removed, followed by feeding them a high phosphate diet for a duration of 3 months. **b.** Blood serum creatinine levels in Ctrl mice (n = 4), Sham mice (n = 4), and CKD mice (n = 4). **c.** Blood urea nitrogen levels in Ctrl mice (n = 4), Sham mice (n = 4), and CKD (n = 4) mice. **d.** Representative micrographs of HE staining and Masson staining of kidney tissues in each group of mice. **e.** Relative mRNA level of NCF2 in each group of mouse kidney tissue. **f.** Relative mRNA level of S100A9 in each group of mouse kidney tissue. **g.** Relative mRNA level of SELL in each group of mouse kidney tissue. **h.** Western blotting was used to detect expression of NCF2, S100A9, and SELL in kidney tissues from Ctrl mice (n = 4), Sham mice (n = 4), and CKD (n = 4) mice. **i.** Quantitative analysis of NCF2, S100A9, and SELL expression in kidney tissues from Ctrl mice (n = 4), Sham mice (n = 4), and CKD (n = 4) mice. **j.** Immunohistochemistry staining of NCF2, S100A9, and SELL in each group mouse kidney tissues.

4. Discussion

CKD is characterized by persistent structural or functional abnormalities in the kidneys lasting for more than three months, arising from diverse etiologies [1]. It is accompanied by a grim prognosis and a protracted disease course. In recent years, the global prevalence of CKD as a leading cause of death has been steadily increasing, primarily attributed to the accelerated aging of the population, making it a prominent public health concern [18,19]. Timely detection and intervention in CKD can effectively slow down the decline in renal function and curtail the overall cost of treatment [20]. The utilization of potential diagnostic biomarkers for CKD to identify high-risk populations susceptible to morbidity and mortality is conducive to early recognition and proactive intervention, facilitating the management of underlying pathogenic factors and, consequently, mitigating the onset and progression of CKD. In our research, conducted within the domain of immunology and inflammation, we performed an extensive bioinformatics analysis. For the first time, this analysis led to the identification of DEIOSGs in CKD compared to normal human kidney samples. Furthermore, we uncovered novel biomarkers associated with immunity and inflammation, holding direct implications for CKD. These findings not only enhance our understanding of the underlying mechanisms of CKD but also hold promising potential for the development of innovative therapeutic targets.

This study involved a comprehensive examination of changes in gene expression profiles in the transcriptome by comparing 39 CKD kidney samples to 18 healthy kidney samples, combined with OS-related genes, immune infiltration assessment, and WGCNA. Our comprehensive approach led to the identification of 29 DEIOSGs that exhibited distinct expression in CKD compared to the healthy samples. Afterwards, GO and KEGG enrichment analyses were conducted, the majority of these genes were enriched in biological processes associated with inflammation, including inflammatory response, neutrophil chemotaxis, and positive regulation of inflammatory response. Previous research also indicated that CKD was linked to multiple biological functions associated with inflammation. Inflammation is a pervasive feature in CKD, closely related to oxidative stress, immunity [21,22]. Furthermore, correlation analysis and PPI network analysis were employed to delve deeper into the interplay among DEIOSGs. According to the PPI network

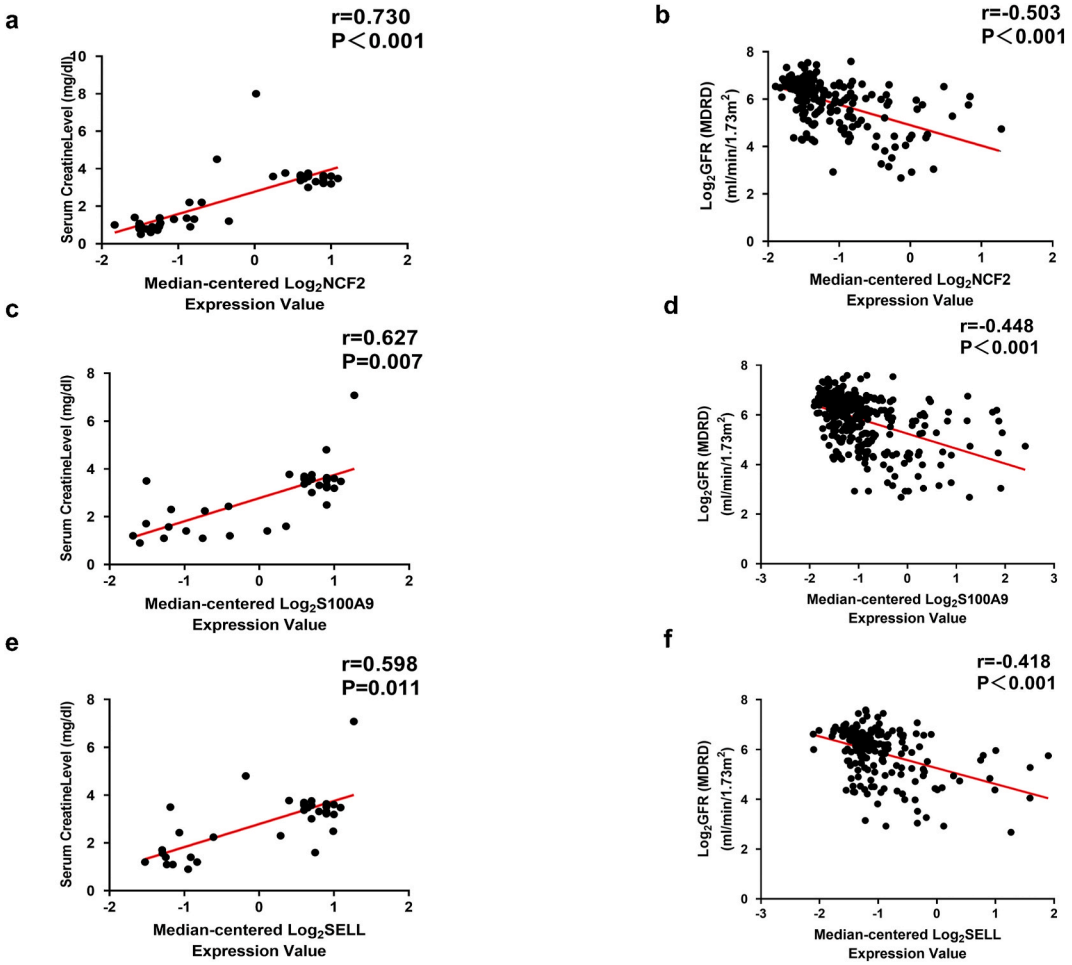

Fig. 7. Associations between the expression of hub genes and key renal functions parameters in the Nephroseq database. a. Correlation between NCF2 expression and blood serum creatinine in the TubInt cohort of IgA nephropathy within Ju CKD ($r = 0.730$, $P < 0.001$). **b.** Correlation between NCF2 expression and GFR in the Ju CKD TubInt cohorts ($r = -0.503$, $P < 0.001$). **c.** Correlation between S100A9 expression and blood serum creatinine in the Ju CKD diabetic nephropathy TubInt cohort ($r = 0.627$, $P = 0.007$). **d.** Correlation between S100A9 expression and GFR in Ju CKD TubInt cohorts ($r = -0.448$, $P < 0.001$). **e.** Correlation between SELL expression and blood serum creatinine in the Ju CKD diabetic nephropathy TubInt cohort ($r = 0.598$, $P = 0.011$). **f.** Correlation between SELL expression and GFR in Ju CKD TubInt cohorts ($r = -0.418$, $P < 0.001$).

analysis, as substantiated by MCODE scores and MCC scores, NCF2, S100A9, and SELL were identified as pivotal hub genes crucial to CKD-related renal injury.

NCF2 assumes a critical role as a cytoplasmic component of NADPH oxidase, involved in the production of reactive oxygen species (ROS) [23]. ROS, encompassing molecules such as H_2O_2, superoxide anion, and hydroxyl radicals, possess the capacity to initiate oxidative modifications in cellular components, including lipids, proteins, and DNA. Prolonged ROS production can result in genetic mutations and the formation of cancerous cells. NCF2 exerts significant influence in microbial phagocytosis and can be associated with chronic granulomatous diseases when subjected to mutations [24]. Furthermore, NCF2 functions as an immune molecule with the potential to modulate anti-tumor immune responses and impact the prognosis of cancer patients. Previous research has explored the influence of NCF2 on outcomes in cancer patients. For instance, in lung cancer, a single nucleotide polymorphism of NCF2 has been linked to prognosis [25]. Within the realm of renal diseases, NCF2 has emerged as a pivotal gene in the context of clear cell renal carcinoma (ccRCC). Its expression is intricately intertwined with tumor immune cell infiltration and holds significance for patient prognosis [26]. Ma et al. [27] have substantiated that NCF2 represents a potential key gene linked to ferritin regulation, actively participating in tubulointerstitial injury among patients with DN. Furthermore, its expression exhibits a negative correlation with GFR in DN patients. Overall, this collection of evidence highlights the possibility of NCF2 serving as a crucial biomarker and therapeutic target in the context of CKD.

S100A9, a prominent member of the S100 family of calcium-binding proteins, is primarily secreted by inflammatory cells, tumor cells, and stromal cells. It exhibits the capability to interact with TLR4 in either a paracrine or autocrine manner, thereby initiating the activation of NLRP3 inflammatory complexes. These inflammatory complexes serve as pivotal components within multi-protein

oligomer structures and innate immune networks, becoming engaged in 'aseptic' inflammatory responses triggered by damage-related molecular patterns (DAMPs) [28,29]. Studies have elucidated that S100A9 not only displays elevated levels in inflammatory conditions like inflammatory bowel disease, systemic lupus erythematosus, and rheumatoid arthritis, but it also exhibits a close association with numerous neurodegenerative diseases of the central nervous system [30–33]. Within the domain of renal diseases, Yang et al. [34] identified the S100a9^{hi}Ly6c^{hi}IMs population as early responders in acute kidney injury (AKI). The mononuclear phagocyte system in a rat model of ischemia-reperfusion injury (IRI) demonstrates the initiation and expansion of renal inflammation, as shown by single-cell RNA sequencing of these cells. At the same time, the presence of S100A8/A9^{+} macrophages in the kidneys and their association with tissue damage were confirmed. Another study highlighted that the serum expression of S100A8/S100A9 in patients can serve as an indicator of disease activity in conditions such as ANCA-related vasculitis and glomerulonephritis [35]. Additionally, inhibiting S100A8/A9 in DN demonstrated the potential to ameliorate renal interstitial fibrosis [36]. Collectively, these results provide strong evidence indicating the involvement of S100A9 in the onset and progression of CKD.

The SELL gene encodes the L-selectin protein, also known as CD62L. This protein serves as a critical cell adhesion molecule within the realm of the immune system, particularly in orchestrating the migration and precise localization of white blood cells [37]. Selectin L finds its predominant expression on the surfaces of leukocytes, encompassing lymphocytes and monocytes. By binding with ligands on the surface of vascular endothelial cells, Selectin L effectively facilitates the rolling, adhesion, and migration of white blood cells. In the context of inflammation and immune responses, it plays a pivotal role in guiding white blood cells to the sites of infection or injury within the body, thereby enabling a robust response to in vivo inflammatory and immune challenges [38]. Alterations in the expression level or genetic variations of the SELL can potentially impact the functionality and expression of the Selectin L protein. Consequently, this can influence the migration and localization of immune cells. These changes have been associated with immune system and inflammation, such as systemic lupus erythematosus and inflammatory bowel disease [39,40]. Notably, in the context of kidney, research has revealed intriguing findings. In a study involving an AKI pig model induced by cardiopulmonary bypass (CPB) heart surgery, it was observed that the gene expression of SELL decreased in the renal medulla [41]. However, Geng et al. [42] confirmed an increase in SELL expression in the renal cortex of DN mice through an analysis of the GEO database and animal experiments. These findings suggest a close association between SELL and the progression of renal diseases.

The hub genes (NCF2, S100A9, and SELL) exhibited exceptional diagnostic utility in distinguishing CKD patients and healthy controls through ROC analysis. This enhanced expression of hub genes was corroborated by the independent data set GSE104948. To validate our findings, a CKD mouse model was constructed via a 5/6 nephrectomy procedure, noting a significant rise in the mRNA and protein levels of NCF2, S100A9, and SELL within the kidneys of CKD mice, while the gene expression in the sham-operated mice did not change significantly. Furthermore, a positive correlation emerged between the expression levels of these hub genes and serum creatinine levels among CKD patients. Moreover, there was a negative correlation between hub genes and GFR. Collectively, hub genes NCF2, S100A9 and SELL may serve as promising biomarkers of CKD related to immune and oxidative stress.

Our research offers a fresh perspective and identifies a promising avenue for future investigations into the intricate interplay between CKD and immune and oxidative stress. It is important to acknowledge, however, that our analysis is constrained by the limited number of available samples. This limitation arises from the scarcity of transcriptome data derived from CKD kidney samples, as well as the diversity of platforms utilized for data collection. To gain a more comprehensive understanding of the potential mechanisms behind the roles of NCF2, S100A9, and SELL in CKD, it is imperative that we expand our data set to include a larger and more diverse pool of samples, alongside enriched clinical information.

5. Conclusions

For the first time, our bioinformatics analysis has successfully identified DEIOSGs within CKD compared to normal human renal samples. Among these DEIOSGs, NCF2, S100A9, and SELL were validated as biomarkers associated with immune response and oxidative stress in CKD. This discovery not only sheds new light on the intricate relationship between CKD and immune and oxidative stress but also presents promising avenues for further research in this domain.

Ethics approval and consent to participate

The study was approved by the Ethics Committee of Qilu Hospital, Shandong University (Approval No: KYLL-2020 (KS) −030).

Consent for publication

All authors consent to publication.

Availability of data and material

All research materials are accessible within the articles and supplementary materials. If further data is needed, please free to request it from us.

Funding

This study was supported by the National Natural Science Foundation of China (No. 82070746, 82270775), the ECCM Program of

the Clinical Research Center of Shandong University (No. 2021SDUCRCB007), the National Science Foundation for Young Scientists of China (Grant No. 82000692), and the Shandong Natural Science Youth Fund (ZR2023QH239).

CRediT authorship contribution statement

Fang Bai: Writing – original draft, Validation, Supervision, Methodology, Data curation, Conceptualization. **Chunjie Wang:** Investigation, Formal analysis, Data curation. **Xin Fan:** Resources, Investigation, Data curation. **Lin Fang:** Validation, Software, Data curation. **Luyao Li:** Visualization, Validation, Software, Data curation. **Xiaoning Zhang:** Investigation, Formal analysis, Data curation. **Kuipeng Yu:** Validation, Methodology, Funding acquisition. **Lei Liu:** Writing – review & editing, Supervision, Methodology. **Ling Guo:** Writing – review & editing, Visualization, Supervision. **Xiangdong Yang:** Writing – review & editing, Supervision, Funding acquisition, Conceptualization.

Declaration of competing interest

We declare that we have no financial and personal relationships with other people or organizations that could inappropriately influence our work, there is no conflict of interest for all authors.

Acknowledgements

Appreciation to all who participated in the article.

Appendix A. Supplementary data

Supplementary data to this article can be found online at https://doi.org/10.1016/j.heliyon.2024.e27754.

References

[1] A.C. Webster, E.V. Nagler, R.L. Morton, P. Masson, Chronic kidney disease, Lancet 389 (10075) (2017) 1238–1252.
[2] J.S. Lees, C.E. Welsh, C.A. Celis-Morales, D. Mackay, J. Lewsey, S.R. Gray, et al., Glomerular filtration rate by differing measures, albuminuria and prediction of cardiovascular disease, mortality and end-stage kidney disease, Nat Med 25 (11) (2019) 1753–1760.
[3] O. Harari-Steinberg, S. Metsuyanim, D. Omer, Y. Gnatek, R. Gershon, S. Pri-Chen, et al., Identification of human nephron progenitors capable of generation of kidney structures and functional repair of chronic renal disease, EMBO Mol. Med. 5 (10) (2013) 1556–1568.
[4] R. Huang, P. Fu, L. Ma, Kidney fibrosis: from mechanisms to therapeutic medicines, Signal Transduct Target Ther 8 (1) (2023) 129.
[5] Q. Yuan, B. Tang, C. Zhang, Signaling pathways of chronic kidney diseases, implications for therapeutics, Signal Transduct Target Ther 7 (1) (2022) 182.
[6] K. Daenen, A. Andries, D. Mekahli, A. Van Schepdael, F. Jouret, B. Bammens, Oxidative stress in chronic kidney disease, Pediatr. Nephrol. 34 (6) (2019) 975–991.
[7] T. Ebert, O. Neytchev, A. Witasp, K. Kublickiene, P. Stenvinkel, P.G. Shiels, Inflammation and oxidative stress in chronic kidney disease and dialysis patients, Antioxid Redox Signal 35 (17) (2021) 1426–1448.
[8] A. Podkowińska, D. Formanowicz, Chronic kidney disease as oxidative stress- and inflammatory-mediated cardiovascular disease, Antioxidants 9 (8) (2020) 752.
[9] M.V. Irazabal, V.E. Torres, Reactive oxygen species and redox signaling in chronic kidney disease, Cells 9 (6) (2020) 1342.
[10] M. Syed-Ahmed, M. Narayanan, Immune dysfunction and risk of infection in chronic kidney disease, Adv Chronic Kidney Dis 26 (1) (2019) 8–15.
[11] W. Lai, Y. Xie, X. Zhao, X. Xu, S. Yu, H. Lu, et al., Elevated systemic immune inflammation level increases the risk of total and cause-specific mortality among patients with chronic kidney disease: a large multi-center longitudinal study, Inflamm. Res. 72 (1) (2023) 149–158.
[12] M. de Cos, M. Xipell, A. García-Herrera, G.M. Lledo, E. Guillen, M. Blasco, et al., Assessing and counteracting fibrosis is a cornerstone of the treatment of CKD secondary to systemic and renal limited autoimmune disorders, Autoimmun. Rev. 21 (3) (2022) 103014.
[13] T.K. Chen, D.H. Knicely, M.E. Grams, Chronic kidney disease diagnosis and management: a review, JAMA 322 (13) (2019) 1294–1304.
[14] M.E. Ritchie, B. Phipson, D. Wu, Y. Hu, C.W. Law, W. Shi, et al., Limma powers differential expression analyses for RNA-sequencing and microarray studies, Nucleic Acids Res. 43 (7) (2015) e47.
[15] A.M. Newman, C.B. Steen, C.L. Liu, A.J. Gentles, A.A. Chaudhuri, F. Scherer, et al., Determining cell type abundance and expression from bulk tissues with digital cytometry, Nat. Biotechnol. 37 (7) (2019 Jul) 773–782.
[16] P. Langfelder, S. Horvath, WGCNA: an R package for weighted correlation network analysis, BMC Bioinf. 9 (2008) 559.
[17] J. Shi, Y. Yang, Y.N. Wang, Q. Li, X. Xing, A.Y. Cheng, et al., Oxidative phosphorylation promotes vascular calcification in chronic kidney disease, Cell Death Dis. 13 (3) (2022) 229.
[18] C. Yang, H. Wang, X. Zhao, K. Matsushita, J. Coresh, L. Zhang, et al., CKD in China: evolving spectrum and public health implications, Am. J. Kidney Dis. 76 (2) (2020) 258–264.
[19] L. Wang, X. Xu, M. Zhang, C. Hu, X. Zhang, C. Li, et al., Prevalence of chronic kidney disease in China: results from the sixth China chronic disease and risk factor surveillance, JAMA Intern. Med. 183 (4) (2023) 298–310.
[20] M.G. Shlipak, S.L. Tummalapalli, L.E. Boulware, M.E. Grams, J.H. Ix, V. Jha, et al., The case for early identification and intervention of chronic kidney disease: conclusions from a Kidney Disease: improving Global Outcomes (KDIGO) Controversies Conference, Kidney Int. 99 (1) (2021) 34–47.
[21] F. Graterol Torres, M. Molina, J. Soler-Majoral, G. Romero-González, N. Rodríguez Chitiva, M. Troya-Saborido, et al., Evolving concepts on inflammatory biomarkers and malnutrition in chronic kidney disease, Nutrients 14 (20) (2022) 4297.
[22] M. Diaz-Ricart, S. Torramade-Moix, G. Pascual, M. Palomo, A.B. Moreno-Castaño, J. Martinez-Sanchez, et al., Endothelial damage, inflammation and immunity in chronic kidney disease, Toxins 12 (6) (2020) 361.
[23] E. Tarazona-Santos, M. Machado, W.C. Magalhães, R. Chen, F. Lyon, L. Burdett, A. Crenshaw, et al., Evolutionary dynamics of the human NADPH oxidase genes CYBB, CYBA, NCF2, and NCF4: functional implications, Mol. Biol. Evol. 30 (9) (2013) 2157–2167.
[24] I.L. Roth, P. Salamon, T. Freund, Y.B. Gadot, S. Baron, T. Hershkovitz, et al., Novel NCF2 mutation causing chronic granulomatous disease, J. Clin. Immunol. 40 (7) (2020) 977–986.

[25] S. Yang, D. Tang, Y.C. Zhao, H. Liu, S. Luo, T.E. Stinchcombe, et al., Potentially functional variants of ERAP1, PSMF1 and NCF2 in the MHC-I-related pathway predict non-small cell lung cancer survival, Cancer Immunol. Immunother. 70 (10) (2021) 2819–2833.
[26] G.M. Chalbatani, S.A. Momeni, M.H. Mohammadi Hadloo, Z. Karimi, M. Hadizadeh, S.A. Jalali, et al., Comprehensive analysis of ceRNA networks to determine genes related to prognosis, overall survival, and immune infiltration in clear cell renal carcinoma, Comput. Biol. Med. 141 (2022) 105043.
[27] L.L. Ma, Y. Bai, W.H. Liu, Z.L. Diao, Bioinformatics analysis of potential key ferroptosis-related genes involved in tubulointerstitial injury in patients with diabetic nephropathy, Ren. Fail. 45 (1) (2023) 2199095.
[28] Y. He, H. Hara, G. Núñez, Mechanism and regulation of NLRP3 inflammasome activation, Trends Biochem. Sci. 41 (12) (2016) 1012–1021.
[29] D.E. Place, T.D. Kanneganti, Recent advances in inflammasome biology, Curr. Opin. Immunol. 50 (2018) 32–38.
[30] S. Su, W. Kong, J. Zhang, X. Wang, H. Guo, Integrated analysis of DNA methylation and gene expression profiles identified S100A9 as a potential biomarker in ulcerative colitis, Biosci. Rep. 40 (12) (2020) BSR20202384.
[31] A.J. Monteith, J.M. Miller, J.M. Williams, K. Voss, J.C. Rathmell, L.J. Crofford, et al., Altered mitochondrial homeostasis during systemic lupus erythematosus impairs neutrophil extracellular trap formation rendering neutrophils ineffective at combating Staphylococcus aureus, J. Immunol. 208 (2) (2022) 454–463.
[32] J. Inciarte-Mundo, B. Frade-Sosa, R. Sanmartí, From bench to bedside: calprotectin (S100A8/S100A9) as a biomarker in rheumatoid arthritis, Front. Immunol. 13 (2022) 1001025.
[33] X. Zhang, D. Sun, X. Zhou, C. Zhang, Q. Yin, L. Chen, Y. Tang, et al., Proinflammatory S100A9 stimulates TLR4/NF-κB signaling pathways causing enhanced phagocytic capacity of microglial cells, Immunol. Lett. 255 (2023) 54–61.
[34] W. Yao, Y. Chen, Z. Li, J. Ji, A. You, S. Jin, et al., Single cell RNA sequencing identifies a unique inflammatory macrophage subset as a druggable target for alleviating acute kidney injury, Adv. Sci. 9 (12) (2022) e2103675.
[35] R.J. Pepper, S. Hamour, K.M. Chavele, S.K. Todd, N. Rasmussen, S. Flint, et al., Leukocyte and serum S100A8/S100A9 expression reflects disease activity in ANCA-associated vasculitis and glomerulonephritis, Kidney Int. 83 (6) (2013) 1150–1158.
[36] L. Du, Y. Chen, J. Shi, X. Yu, J. Zhou, X. Wang, et al., Inhibition of S100A8/A9 ameliorates renal interstitial fibrosis in diabetic nephropathy, Metabolism 144 (2023) 155376.
[37] A. Ivetic, H.L. Hoskins Green, S.J. Hart, L-Selectin: a major regulator of leukocyte adhesion, migration and signaling, Front. Immunol. 10 (2019) 1068.
[38] S. Wedepohl, F. Beceren-Braun, S. Riese, K. Buscher, S. Enders, G. Bernhard, et al., L-selectin–a dynamic regulator of leukocyte migration, Eur. J. Cell Biol. 91 (4) (2012) 257–264.
[39] J. Font, P. Pizcueta, M. Ramos-Casals, R. Cervera, M. García-Carrasco, M. Navarro, et al., Increased serum levels of soluble L-selectin (CD62L) in patients with active systemic lupus erythematosus (SLE), Clin. Exp. Immunol. 119 (1) (2000) 169–174.
[40] F. Bravo, J.A. Macpherson, E. Slack, N. Patuto, J. Cahenzli, K.D. McCoy, et al., Prospective validation of CD-62l (L-Selectin) as marker of durable response to infliximab treatment in patients with inflammatory bowel disease: a 5-year clinical follow-up, Clin. Transl. Gastroenterol. 12 (2) (2021) e00298.
[41] M.T. Ghorbel, N.N. Patel, M. Sheikh, G.D. Angelini, M. Caputo, G.J. Murphy, Changes in renal medulla gene expression in a pre-clinical model of post cardiopulmonary bypass acute kidney injury, BMC Genom. 15 (1) (2014) 916.
[42] X.D. Geng, W.W. Wang, Z. Feng, R. Liu, X.L. Cheng, W.J. Shen, et al., Identification of key genes and pathways in diabetic nephropathy by bioinformatics analysis, J Diabetes Investig 10 (4) (2019) 972–984.